Supplementary Information to: Intrinsic Point Defects and Frenkel Pair Formation in Photovoltaic Absorber Zn_3P_2: Regulating *p*-type Conductivity

Nico Kawashima, Silvana Botti

June 8, 2026

1 Pristine lattice constants

The structural properties of the pristine Zn_3P_2 unit cell were established by relaxing the lattice and the ionic positions using different exchange-correlation functionals and fitting the resulting energies to the Birch–Murnaghan equation of state [1, 2], see Fig. SI1. The resulting ground state properties, highlighting the sensitivity to the choice of functional and motivating the selection of PBEsol for subsequent calculations, are summarized in Table SI1. We chose to proceed with the PBEsol-optimized model. This choice stems from the well-documented tendency of LDA to overbind, leading to an underestimation of lattice parameters, and a similar tendency of PBE to overestimate cell dimensions.

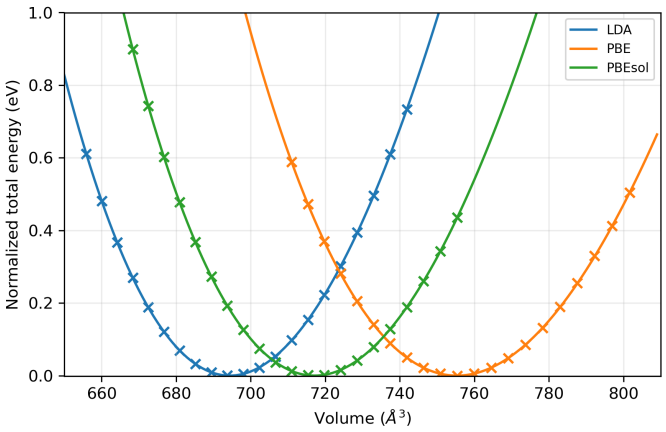

Figure SI1 Total energy as a function of volume computed using LDA, PBE, and PBEsol. Markers denote calculated data points, while solid lines show fits to the Birch-Murnaghan equation of state. Energies are normalized such that the minimum of each fit is set to zero.

Table SI1 Structural properties and Equation of State (EOS) parameters of the 40-atom Zn_3P_2 unit cell calculated using various exchange-correlation functionals. Lattice constants (a, c) and the c/a ratio are compared with available literature values. Reference data are followed by the respective functional used in the cited study in brackets. The cohesive energy E_c is referenced here to spin-polarised free atoms (including atomic spin-polarisation corrections).

Method	a (A)	c (A)	c/a	B_0 (GPa)	B_0'	E_c/atom (eV)
LDA	7.898	11.130	1.409	82.2	4.80	3.096
PBEsol	7.982	11.255	1.410	76.2	5.21	2.671
PBE	8.119	11.457	1.411	64.2	5.06	2.255
Lit. (Theory)	8.029	11.336	1.412 (PBE) [3]			
	8.108	11.416	1.408 (PBE) [4]			
	8.076	11.388	1.410 (HSE) [5]			
	8.080	11.380	1.408 (HSE) [6]			
	8.160	11.342	1.390 (HSE) [4]			
Lit. (Expt.)	8.097	11.450	1.414 [7]			
	8.0785	11.3966	1.4107 [8]			
	8.02	11.67	1.46 [9]			

2 Regarding the errors reported for the effective masses

In principle, effective masses can be obtained by fitting a parabolic function to the electronic band dispersion in the vicinity of a band extremum at a high-symmetry point, along a given crystallographic direction. The effective mass m^* is then extracted from the curvature of the band according to

$$\frac{1}{m^*} = \frac{1}{\hbar^2} \frac{\partial^2 E(k)}{\partial k^2}, \tag{1}$$

where $E(k)$ is the band energy and $\hbar$ is the reduced Planck's constant.

In practice, however, the numerical determination of effective masses involves several methodological choices that can significantly influence the resulting values, particularly for bands with small curvature (heavy electrons or holes). One key parameter is the size of the k-space window around the band extremum, which must be chosen small enough to avoid non-parabolic features of the dispersion, yet large enough to allow for a numerically stable fit. Additional ambiguity arises from the choice of fitting function. While a second-order polynomial is sufficient in theory, higher-order fits are sometimes employed to improve robustness with respect to finite k-point sampling. Furthermore, different fitting strategies may either allow all polynomial coefficients to vary freely or constrain lower-order terms, such as fixing the band-edge energy right at the high-symmetry point to its computed value.

To account for these sources of uncertainty, and given that we find no single fitting protocol can be regarded as uniquely optimal, we evaluated a set of eight different fitting schemes. Specifically, we performed fits using either the ten k-points closest to the band extremum (see Fig. 3 of the main work) or only the five closest points. For each of these two data sets, four fitting functions were considered: (i) a second-order polynomial with all coefficients treated as free parameters, (ii) a third-order polynomial with all coefficients free, (iii) a second-order polynomial in which only the quadratic coefficient was fitted while the two lower-order terms were fixed, and (iv) a third-order polynomial in which only the quadratic and cubic coefficients were fitted.

The effective masses reported in this work correspond to the average over all eight fitting schemes. The associated uncertainties are defined by the maximum deviation of the individual results from this average, i.e., the difference between the average value and the smallest or largest effective mass obtained across all fitting approaches. This procedure provides a conservative estimate of the uncertainty arising from the numerical extraction of effective masses.

3 Influence of exchange–correlation functional and spin–orbit coupling on effective masses

To assess the robustness of the effective masses reported in the main text, we evaluated the influence of the explicit inclusion of spin-orbit coupling (SOC), and the choice of exchange-correlation functional. For that purpose, we performed a complementary calculation in which SOC was neglected, as well as a calculation using the PBE functional.

The resulting band structures close to the band gap at Γ are shown in Fig. SI2 and corresponding effective masses are listed in Table SI2 for direct comparison. We observe that spin-orbit coupling has a significant impact on the electronic structure near the band extrema, leading to band splitting and modified curvatures that directly influence the effective

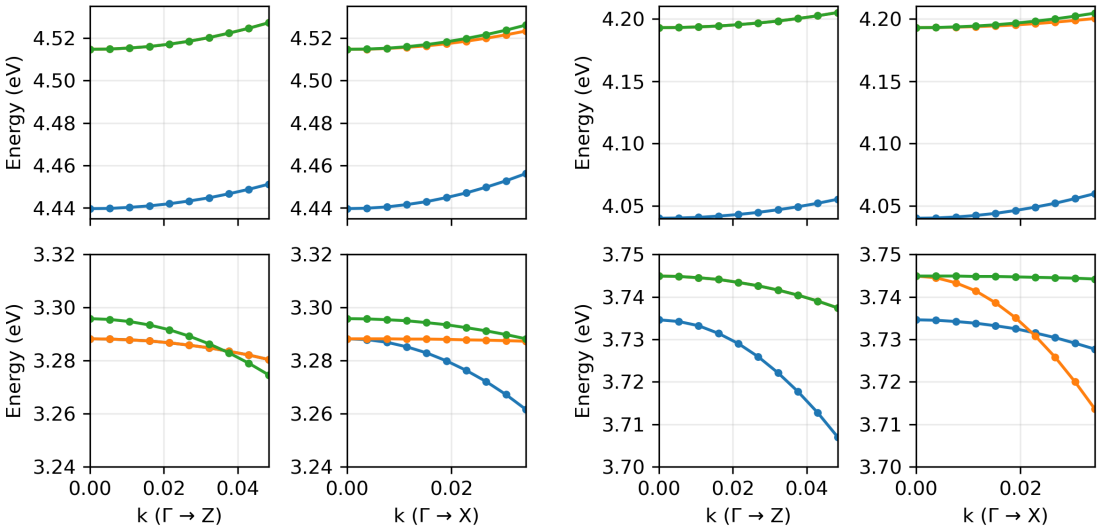

Figure SI2 Electronic band structures near the valence- and conduction-band edges around the Γ point. Left: HSE06 calculations without spin-orbit coupling. Right: PBE calculations without spin-orbit coupling. Effective masses reported in Table SI2 were extracted by fitting the band curvature in the immediate vicinity of Γ.

masses. Neglecting SOC therefore introduces additional quantitative errors. Furthermore, we find that the use of the PBE functional leads to noticeable deviations in the band curvatures compared to HSE06. These differences are accompanied by the well-known underestimation of the band gap within PBE.

Based on these observations, we conclude that the effective masses reported in the main text, obtained using the HSE06 functional with explicit inclusion of spin-orbit coupling, provide the most reliable description within the present computational framework. The additional results presented here serve to illustrate the sensitivity of effective masses to methodological choices and to justify the approach adopted in the main work.

Table SI2 Effective carrier masses at the Γ point computed using different exchange-correlation functionals (HSE06 and PBE) and with or without spin-orbit coupling (wSOC, woSOC). For reference, the values reported in the main text correspond to the HSE06 calculations including spin-orbit coupling (HSE06, wSOC).

path	band	m^* (HSE06, wSOC)	m^* (HSE06, woSOC)	m^* (PBE, woSOC)
$\Gamma \rightarrow$ X	VB3	-0.26 ± 0.09	-0.10 ± 0.01	-0.44 ± 0.10
	VB2	-0.24 ± 0.10	< -2.4	-0.09 ± 0.01
	VB1	-0.50 ± 0.20	-0.38 ± 0.03	< -3.8
	CB1	0.17 ± 0.01	0.17 ± 0.01	0.14 ± 0.01
	CB2	0.28 ± 0.02	0.33 ± 0.06	0.46 ± 0.10
	CB3	0.27 ± 0.02	0.24 ± 0.04	0.23 ± 0.01
$\Gamma \rightarrow$ Z	VB3	-0.31 ± 0.09	-0.47 ± 0.13	-0.10 ± 0.01
	VB2	-0.35 ± 0.01	-0.47 ± 0.13	-0.39 ± 0.02
	VB1	-0.16 ± 0.02	-0.14 ± 0.01	-0.39 ± 0.02
	CB1	0.31 ± 0.09	0.23 ± 0.02	0.18 ± 0.01
	CB2	0.27 ± 0.05	0.23 ± 0.02	0.22 ± 0.02
	CB3	0.27 ± 0.05	0.23 ± 0.02	0.22 ± 0.02

4 Formation energies of various defects computed in this work

This section provides the comprehensive numerical data for the intrinsic defect calculations presented in the main text. Tabulated values include raw energy differences (ΔE), finite-size supercell corrections (E_{corr}), and final formation energies (E^{form}) for all investigated charge states. To facilitate the exact reconstruction of the transition energy diagrams, these data should be used in combination with the chemical potentials defined in the manuscript and the computed valence band maximum (VBM) of 3.289 eV.

As shown, certain defect–charge state combinations exhibit an exceedingly high Kumagai–Oba correction uncertainty (ΔE_{corr}) beyond 50 meV. These elevated uncertainties are primarily associated with unstable or shallow defect states, which are intrinsically difficult to model within the periodic supercell approach. In this study, such instances correspond to highly charged species (e.g., P_i in charge state ±5) that possess significantly higher formation energies than the dominant defect species. Given their negligible thermodynamic concentrations and the convergence limitations of the supercell model for these states, these entries were excluded from further refinement and the resulting transition level analysis.

Table SI3 Detailed breakdown of the energy components used to calculate the formation energies (E^{form}) of intrinsic defects in Zn_3P_2. All values are reported in eV. Following the doped convention, inequivalent defect sites are uniquely identified by their point group symmetry and nearest-neighbor distance. The here reported values for E^{form} are calculated at the P-rich stability limit with the Fermi level set to 0.12 eV above the valence band maximum (VBM). ΔE is the raw DFT energy difference between the defect and host supercells. E_{corr} is the finite-size supercell charge correction (Kumagai-Oba). ΔE_{corr} represents the estimated error in the charge correction based on the potential sampling variance.

Defect	Charge State	ΔE	E_{corr}	ΔE_{corr}	E^{form}
v_Zn_Cs_P2.32	+1	0.275	-0.135	0.011	2.098
v_Zn_Cs_P2.32	±0	3.229	0.000	0.000	1.779
v_Zn_Cs_P2.32	-1	6.308	0.156	0.005	1.605
v_Zn_Cs_P2.32	-2	9.393	0.327	0.012	1.452
v_Zn_Cs_P2.35P2.38P2.70a	+1	0.264	-0.133	0.010	2.089
v_Zn_Cs_P2.35P2.38P2.70a	±0	3.162	0.000	0.000	1.711
v_Zn_Cs_P2.35P2.38P2.70a	-1	6.201	0.129	0.007	1.471
v_Zn_Cs_P2.35P2.38P2.70a	-2	9.275	0.252	0.017	1.259
v_Zn_Cs_P2.35P2.38P2.70b	+1	0.564	-0.153	0.010	2.369
v_Zn_Cs_P2.35P2.38P2.70b	±0	3.470	0.000	0.000	2.019
v_Zn_Cs_P2.35P2.38P2.70b	-1	6.504	0.157	0.007	1.802
v_Zn_Cs_P2.35P2.38P2.70b	-2	9.554	0.314	0.015	1.599
v_P_C2_Zn2.38	+3	-0.823	-0.325	0.032	2.237
v_P_C2_Zn2.38	+2	2.074	-0.228	0.015	1.823
v_P_C2_Zn2.38	+1	4.966	-0.117	0.005	1.416

v_P_C2_Zn2.38	±0	8.951	0.000	0.000	2.110
v_P_C2_Zn2.38	-1	12.654	0.153	0.013	2.557
v_P_C2v_Zn2.32Zn2.35Zn2.70a	+3	-1.017	-0.355	0.032	2.013
v_P_C2v_Zn2.32Zn2.35Zn2.70a	+2	1.853	-0.229	0.018	1.601
v_P_C2v_Zn2.32Zn2.35Zn2.70a	+1	4.750	-0.113	0.008	1.204
v_P_C2v_Zn2.32Zn2.35Zn2.70a	±0	8.653	0.000	0.000	1.812
v_P_C2v_Zn2.32Zn2.35Zn2.70a	-1	12.151	0.156	0.013	2.057
v_P_C2v_Zn2.32Zn2.35Zn2.70b	+3	-0.928	-0.328	0.032	2.129
v_P_C2v_Zn2.32Zn2.35Zn2.70b	+2	1.933	-0.215	0.017	1.695
v_P_C2v_Zn2.32Zn2.35Zn2.70b	+1	4.832	-0.111	0.007	1.288
v_P_C2v_Zn2.32Zn2.35Zn2.70b	±0	8.656	0.000	0.000	1.815
v_P_C2v_Zn2.32Zn2.35Zn2.70b	-1	12.064	0.145	0.013	1.959
Zn_P_C2v_Zn2.32Zn2.35Zn2.70a	+5	-8.599	0.026	0.072	3.080
Zn_P_C2v_Zn2.32Zn2.35Zn2.70a	+4	-5.687	0.040	0.046	2.598
Zn_P_C2v_Zn2.32Zn2.35Zn2.70a	+3	-2.723	0.031	0.028	2.144
Zn_P_C2v_Zn2.32Zn2.35Zn2.70a	+2	0.882	-0.022	0.016	2.287
Zn_P_C2v_Zn2.32Zn2.35Zn2.70a	+1	4.313	-0.032	0.007	2.299
Zn_P_C2v_Zn2.32Zn2.35Zn2.70a	±0	8.112	0.000	0.000	2.721
Zn_P_C2v_Zn2.32Zn2.35Zn2.70b	+5	-8.440	0.015	0.065	3.229
Zn_P_C2v_Zn2.32Zn2.35Zn2.70b	+4	-5.524	0.021	0.041	2.741
Zn_P_C2v_Zn2.32Zn2.35Zn2.70b	+3	-2.562	-0.005	0.024	2.268
Zn_P_C2v_Zn2.32Zn2.35Zn2.70b	+2	1.008	-0.051	0.015	2.384
Zn_P_C2v_Zn2.32Zn2.35Zn2.70b	+1	4.438	-0.049	0.008	2.406
Zn_P_C2v_Zn2.32Zn2.35Zn2.70b	±0	8.331	0.000	0.000	2.940
Zn_P_C2_Zn2.38	+5	-8.789	0.094	0.072	2.959
Zn_P_C2_Zn2.38	+4	-5.880	0.098	0.044	2.463
Zn_P_C2_Zn2.38	+3	-2.937	0.087	0.025	1.986
Zn_P_C2_Zn2.38	+2	0.623	-0.013	0.013	2.037
Zn_P_C2_Zn2.38	+1	4.216	-0.045	0.007	2.189
Zn_P_C2_Zn2.38	±0	8.071	0.000	0.000	2.680
P_Zn_Cs_P2.32	+3	-14.493	0.535	0.043	1.660
P_Zn_Cs_P2.32	+2	-10.463	0.237	0.030	1.983
P_Zn_Cs_P2.32	+1	-7.348	0.121	0.014	1.573
P_Zn_Cs_P2.32	±0	-2.503	0.000	0.000	2.888
P_Zn_Cs_P2.32	-1	0.971	-0.020	0.011	2.933
P_Zn_Cs_P2.32	-2	5.539	0.035	0.021	4.147
P_Zn_Cs_P2.32	-3	9.777	0.206	0.044	5.147
P_Zn_Cs_P2.32	-4	14.413	0.302	0.070	6.470
P_Zn_Cs_P2.32	-5	19.145	0.320	0.101	7.811
P_Zn_Cs_P2.35P2.38P2.70a	+3	-14.593	0.450	0.031	1.474
P_Zn_Cs_P2.35P2.38P2.70a	+2	-10.547	0.245	0.019	1.907
P_Zn_Cs_P2.35P2.38P2.70a	+1	-7.134	0.079	0.012	1.744
P_Zn_Cs_P2.35P2.38P2.70a	±0	-2.910	0.000	0.000	2.481
P_Zn_Cs_P2.35P2.38P2.70a	-1	0.688	-0.034	0.013	2.636
P_Zn_Cs_P2.35P2.38P2.70a	-2	5.365	-0.003	0.022	3.935
P_Zn_Cs_P2.35P2.38P2.70a	-3	9.245	0.135	0.052	4.543
P_Zn_Cs_P2.35P2.38P2.70a	-4	13.894	0.357	0.071	6.006
P_Zn_Cs_P2.35P2.38P2.70a	-5	18.563	0.631	0.087	7.540
P_Zn_Cs_P2.35P2.38P2.70b	+3	-14.707	0.527	0.040	1.437
P_Zn_Cs_P2.35P2.38P2.70b	+2	-10.245	0.225	0.017	2.189
P_Zn_Cs_P2.35P2.38P2.70b	+1	-7.077	0.102	0.007	1.824
P_Zn_Cs_P2.35P2.38P2.70b	±0	-2.456	0.000	0.000	2.935
P_Zn_Cs_P2.35P2.38P2.70b	-1	1.069	-0.013	0.014	3.038
P_Zn_Cs_P2.35P2.38P2.70b	-2	5.544	0.031	0.023	4.148
P_Zn_Cs_P2.35P2.38P2.70b	-3	9.241	0.217	0.035	4.623
P_Zn_Cs_P2.35P2.38P2.70b	-4	14.128	0.295	0.098	6.179
P_Zn_Cs_P2.35P2.38P2.70b	-5	17.984	0.489	0.143	6.820

Zn_i_C1	+2	-8.107	0.283	0.013	0.444
Zn_i_C1	+1	-3.393	0.120	0.005	1.587
Zn_i_C1	±0	1.327	0.000	0.000	2.777
Zn_i_C2v	+2	-8.097	0.282	0.013	0.454
Zn_i_C2v	+1	-3.401	0.121	0.005	1.580
Zn_i_C2v	±0	1.889	0.000	0.000	3.339
Zn_i_Ci	+2	-7.377	0.288	0.015	1.179
Zn_i_Ci	+1	-2.812	0.104	0.005	2.151
Zn_i_Ci	±0	1.821	0.000	0.000	3.272
Zn_i_Cs_P2.45	+2	-8.098	0.283	0.013	0.453
Zn_i_Cs_P2.45	+1	-3.400	0.121	0.005	1.580
Zn_i_Cs_P2.45	±0	1.327	0.000	0.000	2.778
Zn_i_Cs_Zn2.30	+2	-8.098	0.282	0.013	0.453
Zn_i_Cs_Zn2.30	+1	-3.403	0.121	0.005	1.577
Zn_i_Cs_Zn2.30	±0	1.325	0.000	0.000	2.776
Zn_i_D2d_Zn2.16	+2	-8.097	0.282	0.013	0.454
Zn_i_D2d_Zn2.16	+1	-3.397	0.120	0.005	1.583
Zn_i_D2d_Zn2.16	±0	1.328	0.000	0.000	2.779
Zn_i_D2d_Zn2.56	+2	-8.123	0.285	0.013	0.431
Zn_i_D2d_Zn2.56	+1	-2.473	0.118	0.005	2.505
Zn_i_D2d_Zn2.56	±0	1.831	0.000	0.000	3.281
P_i_C1	+5	-21.096	1.098	0.085	3.888
P_i_C1	+4	-17.293	0.874	0.062	4.058
P_i_C1	+3	-14.056	0.673	0.045	3.684
P_i_C1	+2	-10.524	0.302	0.015	3.437
P_i_C1	+1	-7.300	0.155	0.007	3.105
P_i_C1	±0	-3.551	0.000	0.000	3.291
P_i_C1	-1	0.165	-0.075	0.010	3.523
P_i_C1	-2	5.081	-0.121	0.017	4.983
P_i_C1	-3	9.872	-0.132	0.036	6.354
P_i_C2v	+5	-21.199	1.074	0.079	3.761
P_i_C2v	+4	-16.779	0.702	0.045	4.399
P_i_C2v	+3	-13.490	0.464	0.028	4.042
P_i_C2v	+2	-10.529	0.304	0.016	3.433
P_i_C2v	+1	-7.311	0.157	0.007	3.097
P_i_C2v	±0	-3.656	0.000	0.000	3.185
P_i_C2v	-1	0.076	-0.078	0.013	3.431
P_i_C2v	-2	4.973	-0.126	0.025	4.871
P_i_C2v	-3	9.869	-0.136	0.037	6.348
P_i_Ci	+5	-21.096	1.097	0.085	3.887
P_i_Ci	+4	-17.064	0.756	0.065	4.170
P_i_Ci	+3	-13.916	0.520	0.046	3.672
P_i_Ci	+2	-10.737	0.355	0.028	3.277
P_i_Ci	+1	-7.135	0.156	0.006	3.271
P_i_Ci	±0	-3.514	0.000	0.000	3.327
P_i_Ci	-1	0.222	-0.059	0.010	3.596
P_i_Ci	-2	5.181	-0.085	0.021	5.119
P_i_Ci	-3	10.147	-0.076	0.037	6.686
P_i_Cs_P2.45	+5	-20.018	0.879	0.097	4.747
P_i_Cs_P2.45	+4	-18.165	0.872	0.085	3.183
P_i_Cs_P2.45	+3	-13.727	0.422	0.047	3.763
P_i_Cs_P2.45	+2	-10.549	0.276	0.030	3.386
P_i_Cs_P2.45	+1	-7.308	0.158	0.007	3.100
P_i_Cs_P2.45	±0	-3.656	0.000	0.000	3.186
P_i_Cs_P2.45	-1	0.075	-0.077	0.012	3.431
P_i_Cs_P2.45	-2	4.972	-0.127	0.025	4.868
P_i_Cs_P2.45	-3	9.870	-0.136	0.037	6.348

P_i_Cs_Zn2.30	+5	-21.286	1.085	0.118	3.684
P_i_Cs_Zn2.30	+4	-18.166	0.887	0.085	3.199
P_i_Cs_Zn2.30	+3	-13.723	0.441	0.030	3.786
P_i_Cs_Zn2.30	+2	-10.527	0.303	0.015	3.435
P_i_Cs_Zn2.30	+1	-7.299	0.156	0.007	3.108
P_i_Cs_Zn2.30	±0	-3.661	0.000	0.000	3.180
P_i_Cs_Zn2.30	-1	0.166	-0.075	0.010	3.523
P_i_Cs_Zn2.30	-2	4.968	-0.122	0.024	4.870
P_i_Cs_Zn2.30	-3	9.873	-0.132	0.036	6.355
P_i_D2d_Zn2.16	+5	-21.283	1.086	0.118	3.689
P_i_D2d_Zn2.16	+4	-18.163	0.887	0.085	3.202
P_i_D2d_Zn2.16	+3	-15.018	0.681	0.060	2.730
P_i_D2d_Zn2.16	+2	-10.920	0.391	0.027	3.130
P_i_D2d_Zn2.16	+1	-7.302	0.156	0.007	3.105
P_i_D2d_Zn2.16	±0	-3.652	0.000	0.000	3.190
P_i_D2d_Zn2.16	-1	0.077	-0.077	0.013	3.432
P_i_D2d_Zn2.16	-2	4.972	-0.126	0.025	4.869
P_i_D2d_Zn2.16	-3	9.869	-0.136	0.036	6.347
P_i_D2d_Zn2.56	+5	-21.288	1.083	0.118	3.681
P_i_D2d_Zn2.56	+4	-18.165	0.887	0.085	3.199
P_i_D2d_Zn2.56	+3	-15.017	0.671	0.059	2.722
P_i_D2d_Zn2.56	+2	-10.528	0.304	0.016	3.435
P_i_D2d_Zn2.56	+1	-7.305	0.157	0.007	3.103
P_i_D2d_Zn2.56	±0	-3.655	0.000	0.000	3.187
P_i_D2d_Zn2.56	-1	0.075	-0.077	0.012	3.431
P_i_D2d_Zn2.56	-2	4.970	-0.126	0.024	4.867
P_i_D2d_Zn2.56	-3	9.870	-0.135	0.037	6.349

5 Defect Transition Levels and Thermodynamic Concentrations

This section provides a detailed tabulation of the thermodynamic transition levels and the corresponding defect concentrations for the intrinsic species in Zn_3P_2 discussed in the main text. The transition levels, denoted as $\varepsilon(q/q')$, represent the Fermi level positions where the formation energies of two charge states q and q' are equal. The concentrations reported in Table SI4 were calculated using the determined formation energies under P-rich growth conditions, assuming an annealing temperature of $T = 650\,\mathrm{K}$ and a quenching/operating temperature of $T = 300\,\mathrm{K}$. Under these specific conditions, the self-consistent Fermi level was determined to be $0.12\,\mathrm{eV}$ above the valence band maximum (VBM).

Table SI4 Calculated thermodynamic transition levels $\varepsilon(q/q')$ and associated total defect concentrations for intrinsic defects in Zn_3P_2. Transition energies are reported in eV relative to the valence band maximum. Concentration were computed for P-rich growth conditions and a Fermi-level of $0.12\,\mathrm{eV}$ above the valence band maximum.

Defect	Charge Transition	Transition Energy (eV)	Total Concentration (cm^{-3})
v_Zn_Cs_P2.35P2.38P2.70b	$\varepsilon(+1,\pm0)$	-0.23	3.29e+13
v_Zn_Cs_P2.35P2.38P2.70b	$\varepsilon(\pm0,-1)$	-0.10	3.29e+13
v_Zn_Cs_P2.35P2.38P2.70b	$\varepsilon(-1,-2)$	-0.08	3.29e+13
v_Zn_Cs_P2.32	$\varepsilon(+1,\pm0)$	-0.20	9.10e+14
v_Zn_Cs_P2.32	$\varepsilon(\pm0,-1)$	-0.05	9.10e+14
v_Zn_Cs_P2.32	$\varepsilon(-1,-2)$	-0.03	9.10e+14
v_Zn_Cs_P2.35P2.38P2.70a	$\varepsilon(+1,\pm0)$	-0.26	2.89e+16
v_Zn_Cs_P2.35P2.38P2.70a	$\varepsilon(\pm0,-1)$	-0.12	2.89e+16
v_Zn_Cs_P2.35P2.38P2.70a	$\varepsilon(-1,-2)$	-0.09	2.89e+16
Zn_i_D2d_Zn2.56	$\varepsilon(+1,\pm0)$	0.90	1.96e+01
Zn_i_Ci	$\varepsilon(+2,+1)$	1.09	2.16e+09
Zn_i_Ci	$\varepsilon(+1,\pm0)$	1.24	2.16e+09
Zn_i_C1	$\varepsilon(+2,+1)$	1.27	6.14e+15
Zn_i_C1	$\varepsilon(+1,\pm0)$	1.32	6.14e+15

v_P_C2_Zn2.38	$\varepsilon(+3,+2)$	-0.29	2.70e+09
v_P_C2_Zn2.38	$\varepsilon(+2,+1)$	-0.29	2.70e+09
v_P_C2_Zn2.38	$\varepsilon(+1,-1)$	0.69	2.70e+09
v_P_C2v_Zn2.32Zn2.35Zn2.70b	$\varepsilon(+3,+2)$	-0.31	1.41e+10
v_P_C2v_Zn2.32Zn2.35Zn2.70b	$\varepsilon(+2,+1)$	-0.29	1.41e+10
v_P_C2v_Zn2.32Zn2.35Zn2.70b	$\varepsilon(+1,-1)$	0.46	1.41e+10
v_P_C2v_Zn2.32Zn2.35Zn2.70a	$\varepsilon(+3,+2)$	-0.29	6.02e+10
v_P_C2v_Zn2.32Zn2.35Zn2.70a	$\varepsilon(+2,+1)$	-0.28	6.02e+10
v_P_C2v_Zn2.32Zn2.35Zn2.70a	$\varepsilon(+1,-1)$	0.55	6.02e+10
P_Zn_Cs_P2.35P2.38P2.70b	$\varepsilon(+3,+1)$	0.31	2.10e+06
P_Zn_Cs_P2.35P2.38P2.70b	$\varepsilon(+1,-1)$	0.73	2.10e+06
P_Zn_Cs_P2.35P2.38P2.70b	$\varepsilon(-1,-3)$	0.87	2.10e+06
P_Zn_Cs_P2.35P2.38P2.70b	$\varepsilon(-3,-5)$	1.26	2.10e+06
P_Zn_Cs_P2.35P2.38P2.70a	$\varepsilon(+3,+1)$	0.26	7.88e+06
P_Zn_Cs_P2.35P2.38P2.70a	$\varepsilon(+1,-1)$	0.57	7.88e+06
P_Zn_Cs_P2.35P2.38P2.70a	$\varepsilon(-1,-5)$	1.41	7.88e+06
P_Zn_Cs_P2.32	$\varepsilon(+3,+1)$	0.08	1.64e+08
P_Zn_Cs_P2.32	$\varepsilon(+1,-1)$	0.80	1.64e+08
P_Zn_Cs_P2.32	$\varepsilon(-1,-3)$	1.23	1.64e+08
P_Zn_Cs_P2.32	$\varepsilon(-3,-4)$	1.44	1.64e+08
Zn_P_C2v_Zn2.32Zn2.35Zn2.70b	$\varepsilon(+5,+4)$	-0.37	3.01e+01
Zn_P_C2v_Zn2.32Zn2.35Zn2.70b	$\varepsilon(+4,+3)$	-0.35	3.01e+01
Zn_P_C2v_Zn2.32Zn2.35Zn2.70b	$\varepsilon(+3,+1)$	0.19	3.01e+01
Zn_P_C2v_Zn2.32Zn2.35Zn2.70b	$\varepsilon(+1,\pm0)$	0.65	3.01e+01
Zn_P_C2v_Zn2.32Zn2.35Zn2.70a	$\varepsilon(+5,+4)$	-0.36	2.18e+02
Zn_P_C2v_Zn2.32Zn2.35Zn2.70a	$\varepsilon(+4,+3)$	-0.33	2.18e+02
Zn_P_C2v_Zn2.32Zn2.35Zn2.70a	$\varepsilon(+3,+1)$	0.20	2.18e+02
Zn_P_C2v_Zn2.32Zn2.35Zn2.70a	$\varepsilon(+1,\pm0)$	0.54	2.18e+02
Zn_P_C2_Zn2.38	$\varepsilon(+5,+4)$	-0.38	3.30e+03
Zn_P_C2_Zn2.38	$\varepsilon(+4,+3)$	-0.36	3.30e+03
Zn_P_C2_Zn2.38	$\varepsilon(+3,+2)$	0.17	3.30e+03
Zn_P_C2_Zn2.38	$\varepsilon(+2,+1)$	0.27	3.30e+03
Zn_P_C2_Zn2.38	$\varepsilon(+1,\pm0)$	0.61	3.30e+03
P_i_D2d_Zn2.16	$\varepsilon(+5,+4)$	-0.38	6.87e-02
P_i_D2d_Zn2.16	$\varepsilon(+4,+3)$	-0.34	6.87e-02
P_i_D2d_Zn2.16	$\varepsilon(+3,\pm0)$	0.27	6.87e-02
P_i_D2d_Zn2.16	$\varepsilon(+0,-1)$	0.37	6.87e-02
P_i_D2d_Zn2.16	$\varepsilon(-1,-2)$	1.56	6.87e-02
P_i_D2d_Zn2.16	$\varepsilon(-2,-3)$	1.60	6.87e-02

References

[1] F. D. Murnaghan. “The Compressibility of Media under Extreme Pressures”. In: *Proceedings of the National Academy of Sciences* 30.9 (Sept. 1944), pp. 244–247. DOI: 10.1073/pnas.30.9.244. URL: https://www.pnas.org/doi/abs/10.1073/pnas.30.9.244 (visited on 02/20/2026).

[2] Francis Birch. “Finite Elastic Strain of Cubic Crystals”. In: *Physical Review* 71.11 (June 1947), pp. 809–824. DOI: 10.1103/PhysRev.71.809. URL: https://link.aps.org/doi/10.1103/PhysRev.71.809 (visited on 02/20/2026).

[3] Nelson Y. Dzade. “First-Principles Insights into the Interface Chemistry between 4-Aminothiophenol and Zinc Phosphide (Zn3P2) Nanoparticles”. In: *ACS Omega* 5.2 (Jan. 2020), pp. 1025–1032. DOI: 10.1021/acsomega.9b02736. URL: https://doi.org/10.1021/acsomega.9b02736 (visited on 06/20/2023).

[4] Steven Demers and Axel van de Walle. “Intrinsic defects and dopability of zinc phosphide”. In: *Physical Review B* 85.19 (May 2012), p. 195208. DOI: 10.1103/PhysRevB.85.195208. URL: https://link.aps.org/doi/10.1103/PhysRevB.85.195208 (visited on 06/21/2023).

[5] Zhenkun Yuan, Yihuang Xiong, and Geoffroy Hautier. “First-principles study of intrinsic and hydrogen point defects in the earth-abundant photovoltaic absorber Zn3P2”. en. In: *Journal of Materials Chemistry A* 11.38 (Oct. 2023), pp. 20592–20600. ISSN: 2050-7496. DOI: 10.1039/D3TA03697A. URL: https://pubs.rsc.org/en/content/articlelanding/2023/ta/d3ta03697a (visited on 11/29/2023).

[6] Wan-Jian Yin and Yanfa Yan. “The electronic properties of point defects in earth-abundant photovoltaic material Zn3P2: A hybrid functional method study”. In: *Journal of Applied Physics* 113.1 (Jan. 2013), p. 013708. ISSN: 0021-8979. DOI: 10.1063/1.4772708. URL: https://doi.org/10.1063/1.4772708 (visited on 06/21/2023).

[7] M. V. Stackelberg and R. Paulus. “Untersuchungen über die Kristallstruktur der Nitride und Phosphide zweiwertiger Metalle”. en. In: *Zeitschrift für Physikalische Chemie* 22B.1 (Mar. 1933), pp. 305–322. ISSN: 2196-7156, 0942-9352. DOI: 10.1515/zpch-1933-2226. URL: https://www.degruyter.com/document/doi/10.1515/zpch-1933-2226/html (visited on 03/27/2024).

[8] I. E. Zanin et al. “Structure of Zn3P2”. en. In: *Journal of Structural Chemistry* 45.5 (Sept. 2004), pp. 844–848. ISSN: 1573-8779. DOI: 10.1007/s10947-005-0067-9. URL: https://doi.org/10.1007/s10947-005-0067-9 (visited on 03/27/2024).

[9] Elias Z. Stutz et al. “Showcasing the optical properties of monocrystalline zinc phosphide thin films as an earth-abundant photovoltaic absorber”. In: *Materials Advances* 3.2 (2022), pp. 1295–1303. DOI: 10.1039/D1MA00922B. URL: https://pubs.rsc.org/en/content/articlelanding/2022/ma/d1ma00922b (visited on 06/21/2023).